



Supplement of

A comprehensive study about the in-cloud processing of nitrate through coupled measurements of individual cloud residuals and cloud water

Guohua Zhang et al.

Correspondence to: Xinhui Bi (bixh@gig.ac.cn)

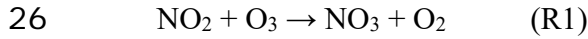
The copyright of individual parts of the supplement might differ from the article licence.

13 **Introduction**

14 Details including the analysis of air masses, meteorological conditions, and
15 characteristics of individual particles over the sampling periods. Text describes the lifetime
16 calculation for NO_x and N₂O₅, and regression and random forest analysis of nitrate
17 production. Tables provide the initial setup of model simulations for nitrate formation in
18 aqueous phase (wet aerosol and cloud droplets). Figures mainly show the characteristics of
19 individual particles, including representative mass spectra and the RPA ratios
20 (nitrate/sulfate) for the identified particle types, distribution of nitrate RPA over cloud free,
21 interstitial, and residual particles, and also the comparison of [NO_x]/[O₃] and SA between
22 cloud events and cloud-free periods.

23 **Text S1 Lifetimes of NO_x and N₂O₅**

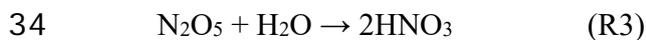
24 The formation of nitrate from hydrolysis of N₂O₅ arises from the reactions between
25 NO₂ and O₃ can be given as follows:



28 Thus, NO_x is converted to N₂O₅ at the following rate ($K_1 = 1.2 \times 10^{-13} \exp(-2450/T)$,
29 T is the absolute temperature), and thus the lifetime of NO_x can be calculated as:

30
$$\tau_{\text{NO}_x} = \frac{1}{2K_1[\text{O}_3]}$$

31 During daytime, NO₃ rapidly photolyzes, but at night, NO₃ reacts with NO₂ to produce
32 N₂O₅. The key reaction to produced condensed nitrate is the hydrolysis of N₂O₅ on aerosol
33 or droplet surfaces:



35 The reaction proceeds effectively on the surface of aerosol particles that contain water.
36 When an N₂O₅ molecule strikes the surface of an aqueous particle, not every collision leads
37 to reaction. A reaction efficiency or uptake coefficient γ was introduced to account for the
38 probability of reaction. Values of γ for this reaction ranging from 0.06 to 0.1 have been
39 reported. The the lifetime of N₂O₅ can be calculated as:

40
$$\tau_{\text{N}_2\text{O}_5} = \left[\frac{\gamma}{4} \left(\frac{8RT}{\pi m_{(\text{N}_2\text{O}_5)}} \right)^{1/2} A_p \right]^{-1}$$
 (Seinfeld and Pandis, 2006)

41 where $\left(\frac{8RT}{\pi m_{(\text{N}_2\text{O}_5)}} \right)^{1/2}$ corresponds to the molecular mean speed of N₂O₅, $m_{(\text{N}_2\text{O}_5)}$ is
42 the molecular mass of N₂O₅, and A_p is the aerosol/droplet surface area (SA) per unit volume
43 ($\text{cm}^2 \text{ cm}^{-3}$). The reaction occurs at a rate governed by that at which N₂O₅ molecules strike
44 the aerosol surface area times the amount of surface area times the reaction efficiency.

45

46 **Text S2 Regression and random forest analysis**

47 As shown in Text S1, the formation of nitrate depends on the $[\text{NO}_x][\text{O}_3]$, SA, and
48 temperature as inputs, and thus could be roughly regressed as follows:

49
$$\text{Nitrate} \sim \exp(-1/T) [\text{O}_3][\text{NO}_2] T^{1/2} A_p$$

50 In the multiple linear model, the least-squares fit is used, and two of the most common
51 measures of model fit are the residual standard error and the proportion of variance
52 explained (R^2). It is noted that A_p (or SA) is not available and thus was not included in the
53 regression for 2018 spring data.

54 Random forest analysis, is for nonlinear multiple regression, using trees as building
55 blocks to construct powerful prediction models (Breiman, 2001). The algorithm first
56 creates multiple decision trees, where each tree is grown by using the bootstrap re-sampling
57 method. The relative importance of the predictor variables can also be obtained, with
58 “Mean Decrease Accuracy” presenting the capability of each independent variable in
59 explaining the variability of SNRs.

60

61 **Text S3 SPAMS**

62 Individual particles are introduced into the SPAMS through a critical orifice. They are
63 focused and accelerated to specific velocities, which can be determined by two continuous
64 diode Nd:YAG laser beams (532 nm) placed downstream. Based on the measured
65 velocities, a pulsed laser (266 nm) is subsequently triggered to desorp/ionize the particles.
66 The generated positive and negative molecular fragments are recorded. The measured
67 velocities are corresponding to d_{va} , based on a calibration using polystyrene latex spheres

68 (PSL, Duke Scientific Corp., Palo Alto) with predefined sizes (0.15-2.0 μm). Peak
69 thresholds were set to record only those peaks with area greater than 5 units to distinguish
70 peaks from the background noise (< 1 unit) in the mass spectra.

71 **TABLES**

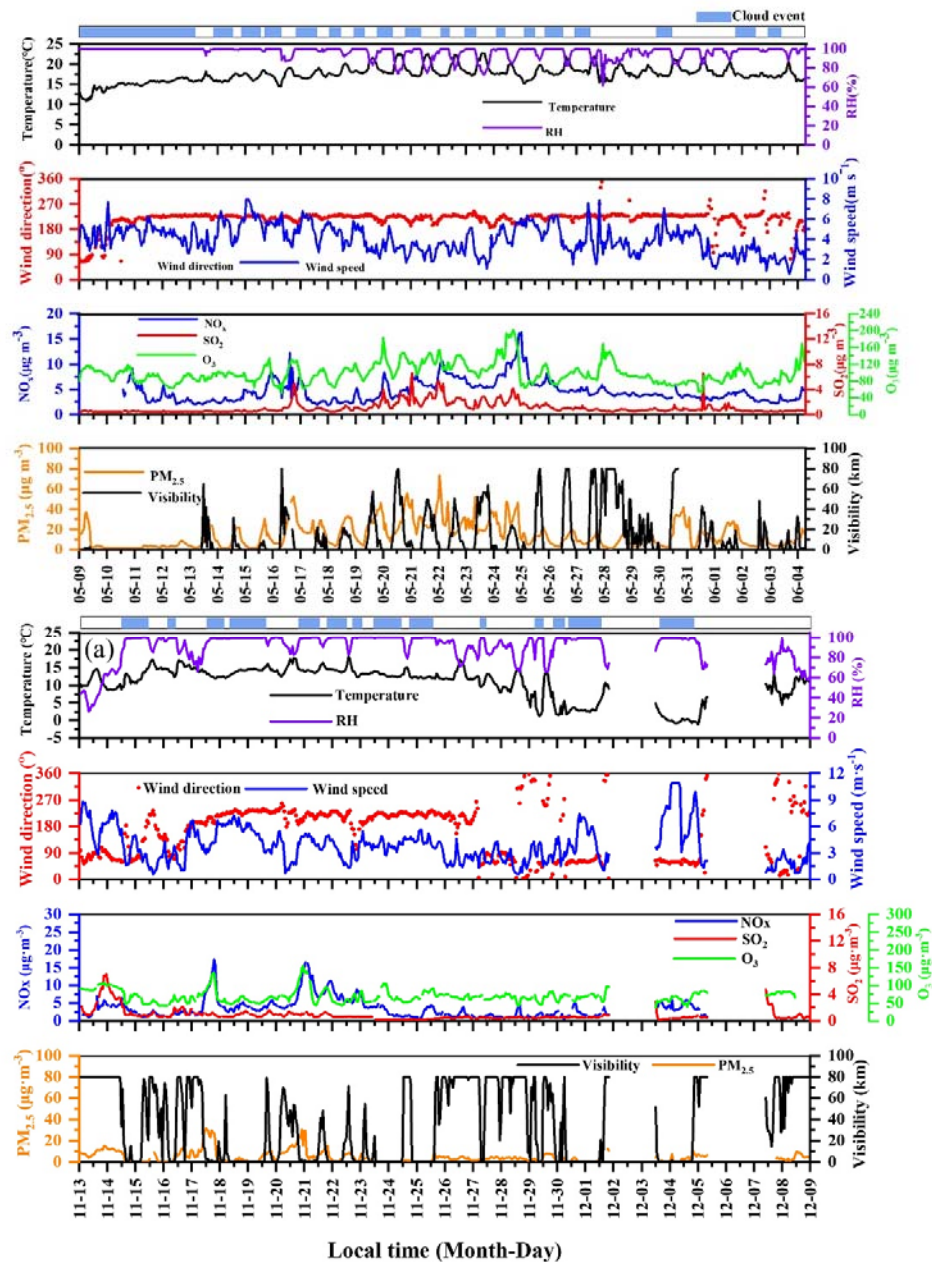
72 Table S1. The initial setup of model simulations for nitrate formation in aqueous phase
 73 (wet aerosol and cloud droplets)

74 In wet aerosol and cloud droplet the RH, LWC, and radius are different, in wet aerosol
 75 case: RH=85% , LWC1= 1.0×10^{-5} g/m³, LWC2= 1.0×10^{-4} g/m³, radius of aerosol particles
 76 is 0.5 μ m; in cloud droplet case: RH=99.99%, LWC1= 0.05 g/m³, LWC2= 0.15 g/m³,
 77 radius of aerosol particles is 8 μ m, and photolysis rate was changed 100%, 50%, and 30%.

78

	Wet aerosol	Wet aerosol	Cloud 1#	Cloud 2#
RH	85%	85%	100%	100%
LWC (g cm⁻³)	10 ⁻⁵	10 ⁻⁴	0.05	0.15
Radius (μ m)	0.5	0.5	8	8
NO ₂ (ppb)	25	25	25	25
O ₃ (ppb)	100	100	100	100
NH ₃ (ppb)	25	25	25	25
HNO ₃ (ppb)	1	1	1	1
photolysis rate (%)	100	100	100; 50; 30	100; 50; 30

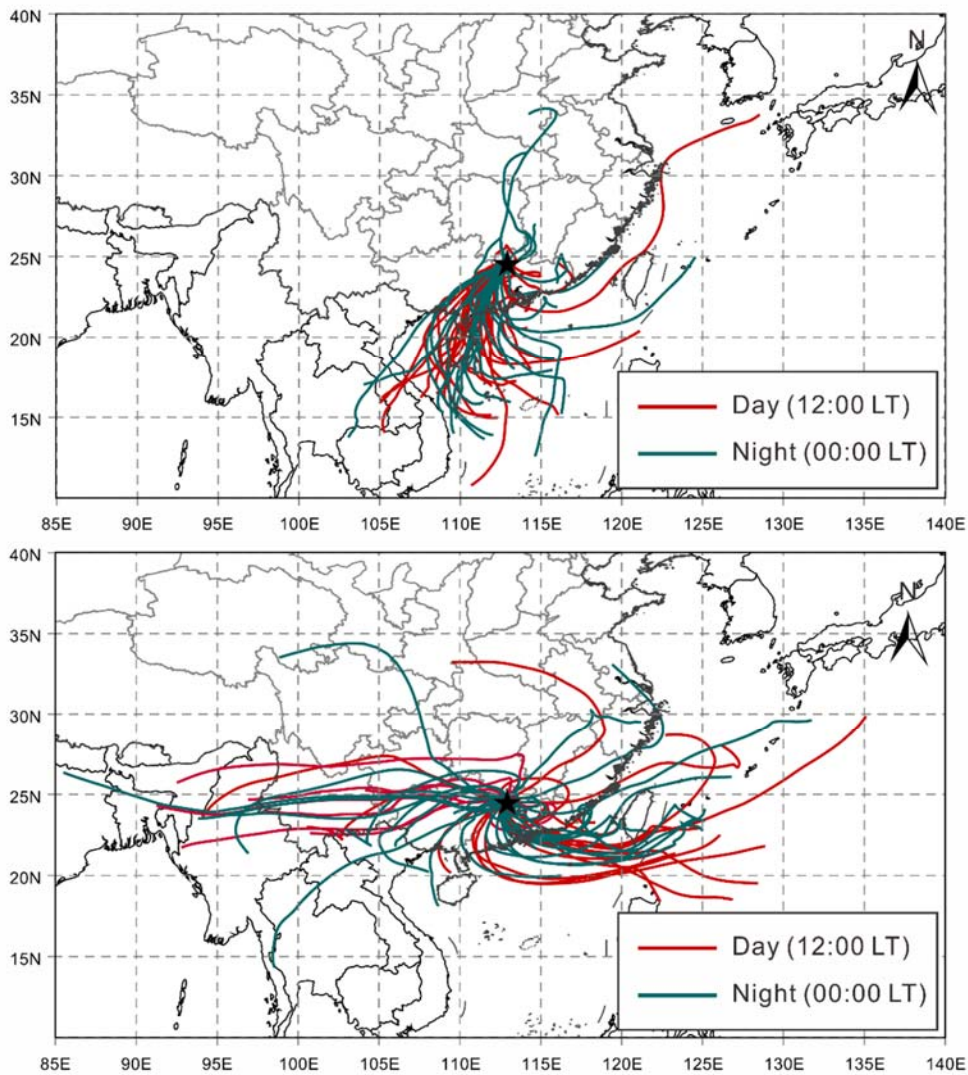
79



80

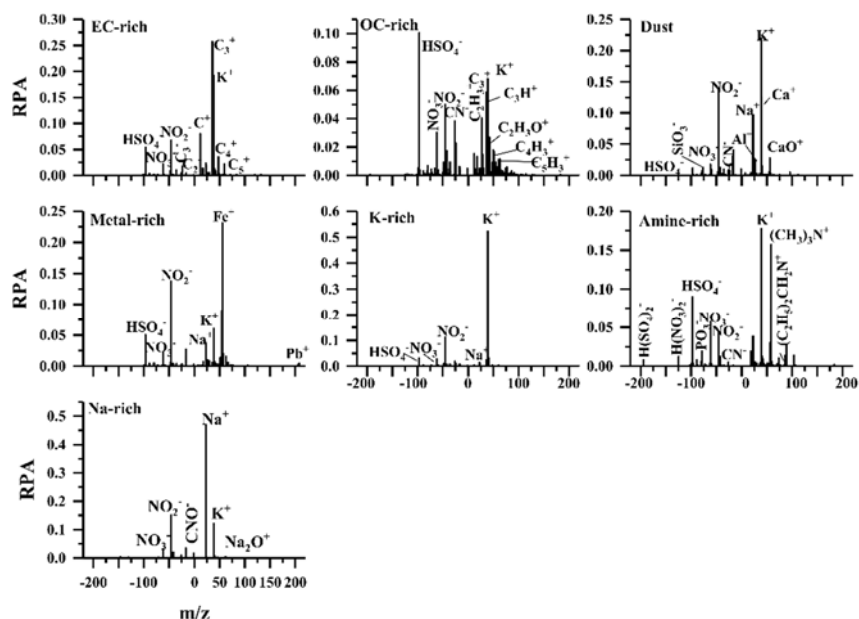
81 **Figure S1.** Temporal variations of T and RH, wind speed and direction, O₃/SO₂/NO_x, and
 82 mass concentration of PM_{2.5} and visibility for 2018 spring (upper) and 2020 winter
 83 (bottom), respectively. Notably, there are unusual temporal patterns for ozone, without the
 84 commonly observed diurnal variations with daytime peak. In addition, the ozone

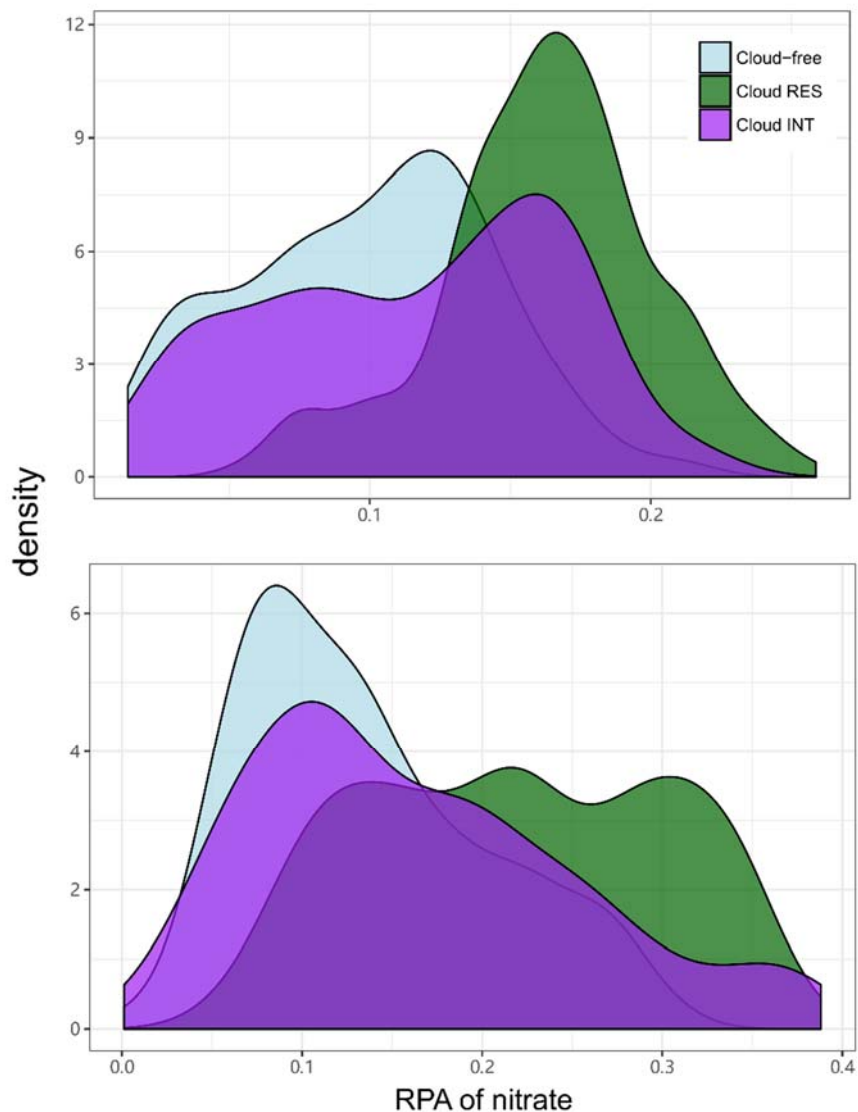
85 concentrations kept at a relatively high level during most of the periods. Given the low
86 NO_x levels ($< 10 \mu\text{g m}^{-3}$), this is likely due to regional transport rather than local formation.
87 This phenomenon is also indicated by an observation conducted at the same site in 2016,
88 where O₃ episodes were associated with high levels of toluene, ethylbenzene, and xylenes
89 transported from industrial regions (Lv et al., 2019).



90

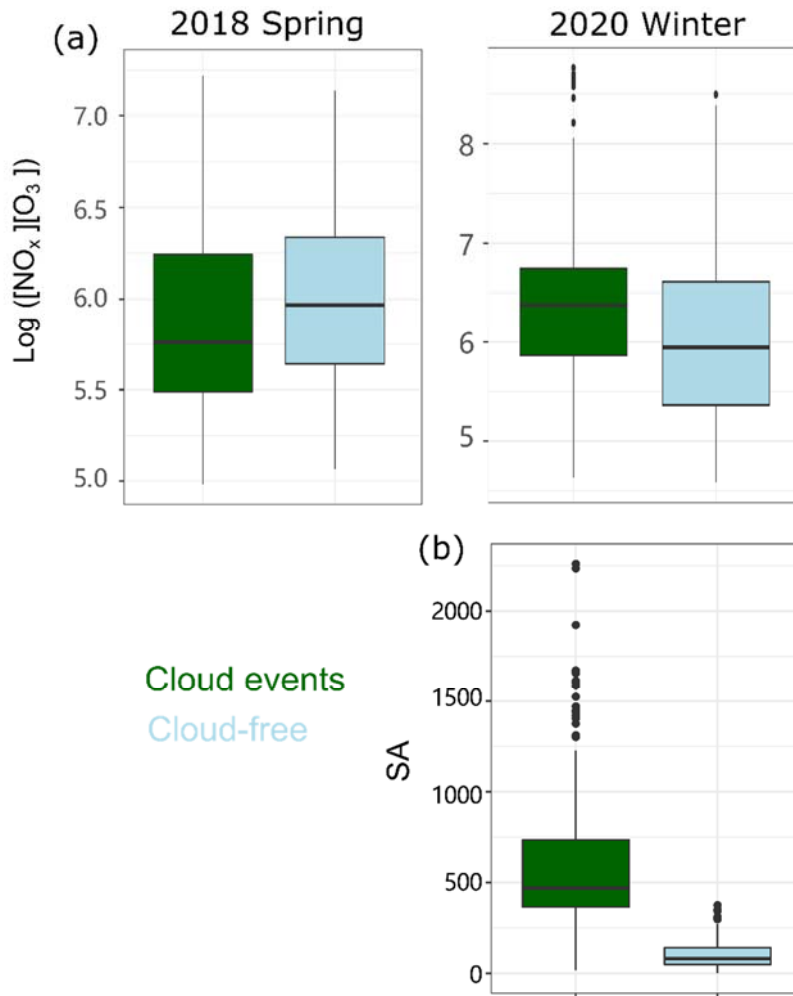
91 **Figure S2.** The HYSPLIT back trajectories (72 h) arriving at the sampling site (100 m
 92 above the sea level) at daytime (12:00 local time, left panel) and nighttime (0:00 local time,
 93 right panel) for 2018 spring (upper) and 2020 winter (bottom), respectively.





105

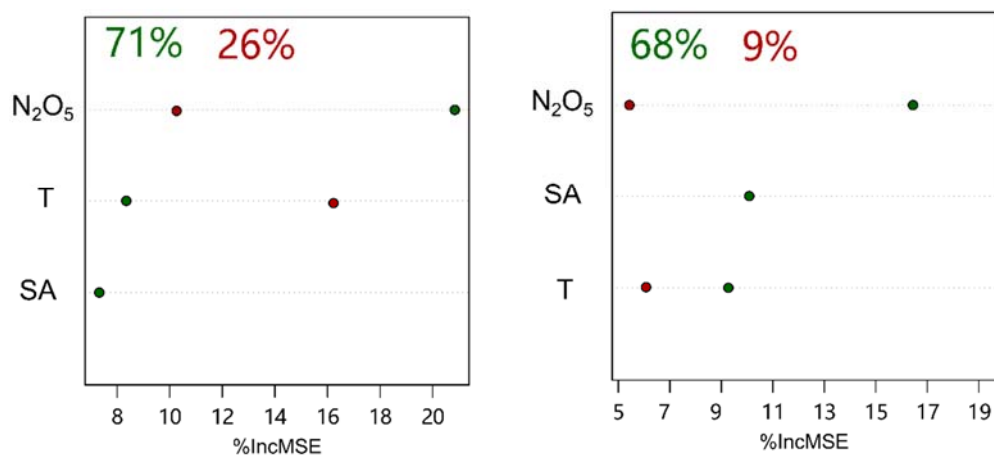
106 **Figure S4.** Distribution of RPA of nitrate, separated for cloud free, INT, and RES
107 particles, in 2018 spring (upper) and 2020 winter (bottom). The RPA of nitrate, as an
108 indicative of the relative abundance of nitrate in the individual particles, was presented
109 in hourly average values. Such distribution shows that the cloud RES particles were
110 associated with higher relative abundance of nitrate, rather than the cloud free particles.



111

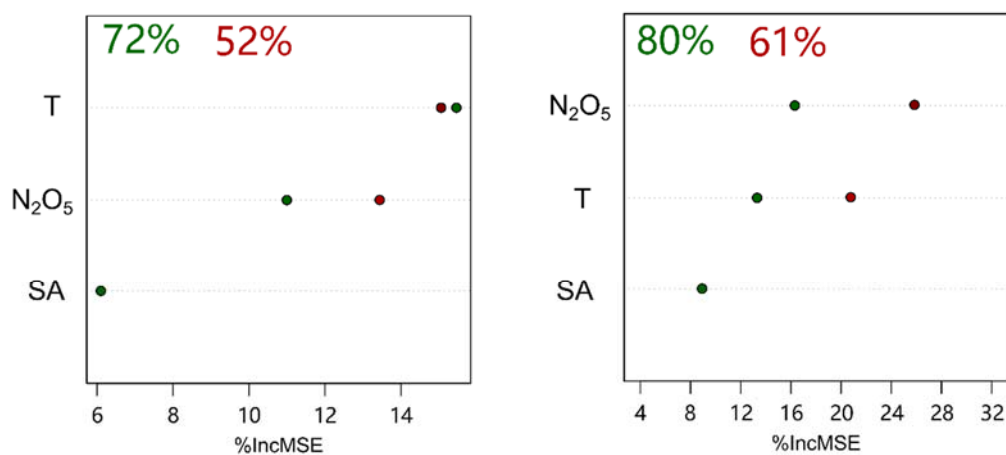
112 **Figure S5.** Box-and-whisker plots of $[\text{NO}_x][\text{O}_3]$ and SA ($\mu\text{m}^2 \text{ cm}^{-3}$) during cloud
 113 events and cloud-free periods in (a) 2018 spring and (b) 2020 winter, respectively.

(a) Cloud-free



(b) Cloud RES

● 2020 Winter ● 2018 Spring

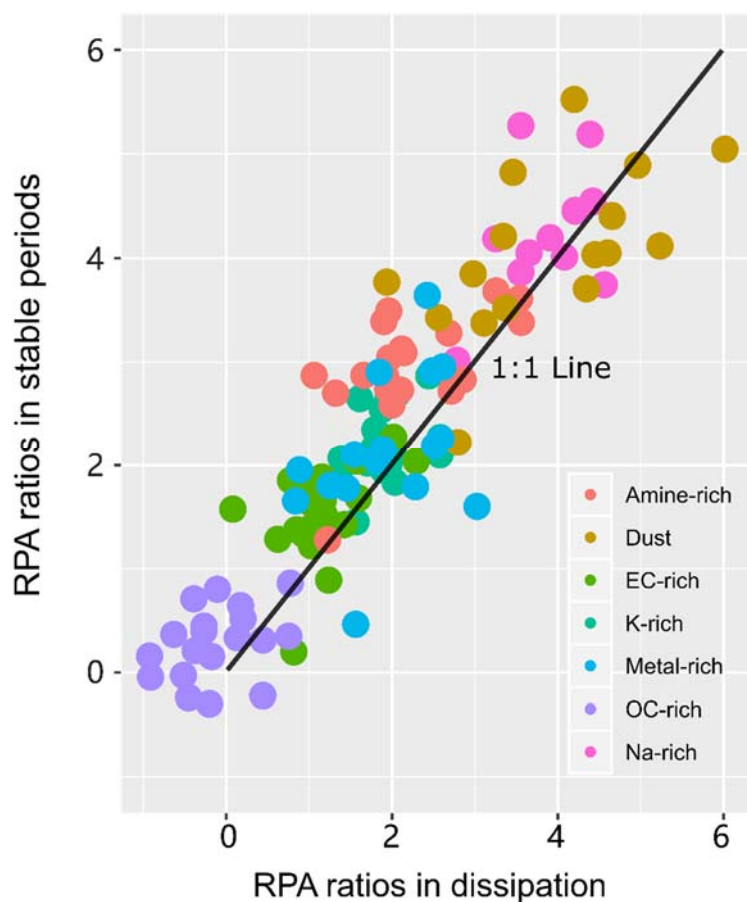


daytime

nighttime

114

115 **Figure S6.** The relative importance of predictors in the random forest analysis for the
116 RPA of nitrate associated with the (a) cloud-free particles and (b) cloud residual
117 particles, respectively, separated for daytime and nighttime during 2018 spring and
118 2020 winter. Used as an indicator for the relative contribution to the predicted
119 variable, %IncMSE refers to the increased mean square-error when each independent
120 variable is removed from the predictors.



121

122 **Figure S7.** The RPA ratios (nitrate/sulfate) varying on the seven single particle types
 123 are compared for mid-cloud and cloud dissipation periods (2h after cloud period) for
 124 2018 spring, which is also similarly observed in 2020 winter. The RPA ratios during
 125 cloud dissipation periods generally follows those in the cloud RES particles during
 126 cloud stable periods. It suggests that the in-cloud produced nitrate remains after cloud
 127 evaporation. It is anticipated that the evaporation of the cloud droplets in the ambient
 128 atmosphere would lead to a level similar to the cloud RES nitrate, and perhaps more if
 129 the ambient relative humidity were higher or the temperature lower than that in the
 130 GCVI (Hayden et al., 2008). As the GCVI is a more severe and rapid approach to the

131 drying of cloud droplets than likely occurs in the atmosphere, the enhanced cloud
132 residual nitrate suggests that when the cloud evaporates, more particulate nitrate than
133 existed in the aerosol below cloud should be released into the air. If this process is
134 significant, an enhancement of nitrate (relative to sulfate) may be expected after cloud
135 evaporation.

136 References

137 Breiman, L.: Random Forests, *Mach. Learn.*, 45, 5-32,

138 doi:10.1023/A:1010933404324, 2001.

139 Hayden, K. L., Macdonald, A. M., Gong, W., Toom-Sauntry, D., Anlauf, K. G.,

140 Leithead, A., Li, S. M., Leitch, W. R., and Noone, K.: Cloud processing of nitrate, *J.*

141 *Geophys. Res.-Atmos.*, 113, 1-18, doi:10.1029/2007jd009732, 2008.

142 Lv, S., Gong, D., Ding, Y., Lin, Y., Wang, H., Ding, H., Wu, G., He, C., Zhou,

143 L., Liu, S., Ristovski, Z., Chen, D., Shao, M., Zhang, Y., and Wang, B.: Elevated

144 levels of glyoxal and methylglyoxal at a remote mountain site in southern China:

145 Prompt in-situ formation combined with strong regional transport, *Sci. Total.*

146 *Environ.*, 672, 869-882, doi:[10.1016/j.scitotenv.2019.04.020](https://doi.org/10.1016/j.scitotenv.2019.04.020), 2019.

147 Seinfeld, J. H., and Pandis, S. N.: *Atmospheric Chemistry and Physics: From Air*

148 *Pollution to Climate Change*, edited by: John Wiley&Sons, I., John Wiley&Sons,

149 Inc., New Jersey, 2006.